Electromotive power generated by pressure gradient in metals with the band Jahn-Teller effect

Mitsuo Kataoka*
Laboratory for Solid State Physics, Moniwadai 2-11-7, Taihaku-ku, Sendai 982-0252, Japan

(Received 24 June 2019; revised 22 March 2022; accepted 9 June 2022; published 27 June 2022)

In band Jahn-Teller (BJT) metals, some lattice distortions with their symmetries different from that of the bulk structure can linearly couple to the BJT electrons, so pressures to produce or enhance such distortions can affect the BJT electrons near the Fermi level. This pressure-electric effect in BJT metals is studied theoretically on the basis of the Γ_{12} subband model for the structural transition in A15 compounds. The applied pressure is assumed to consist of a spatially uniform pressure and a local pressure. The former induces or enhances a uniform distortion, which contributes to the redistribution of electrons between the Γ_{12} subbands, while the latter produces a local distortion with its gradient, which causes flows of band electrons between different regions in space. The steady electronic state under the uniform and local pressures is obtained by use of the Boltzmann equation and the relaxation-time approximation. It is clarified that the local pressure with its gradient can generate an electromotive power when the degeneracy of the BJT subbands is lifted spontaneously and/or by the external uniform pressure. The obtained pressure-gradient electric effect is predicted to be a probe into BJT effects which may work in some metals with structural transitions.

DOI: 10.1103/PhysRevB.105.214112

I. INTRODUCTION

When electronic bands are degenerate in the wave-vector **k** space near the Fermi level ϵ_F in a metal, the metal is sometimes unstable against a bulk structural change. This phenomenon is called the band Jahn-Teller (BJT) effect. An intuitive model for a system consisting of degenerate electronic bands and distortions was presented five decades ago by Labbé and Friedel [1] to explain the origin of cubic-to-tetragonal transitions which occur in some A15 compounds. They assumed that in these compounds, three one-dimensional electronic bands spreading along three orthogonal directions cross the Fermi level ϵ_F in the **k** space, and showed that the total energy of electrons in these bands can be decreased by the tetragonal distortion. However, the later sophisticated band calculation on V_3Si and Nb_3Sn revealed no one-dimensional band but rather doubly degenerate and three-dimensional bands near the Fermi level [2]. On the basis of this band calculation, another BJT model was proposed, in which the doubly degenerate Γ_{12} subbands are responsible for the appearance of the tetragonal distortions in A15 compounds [3,4]. This Γ_{12}-subband model could successfully explain some characteristic properties of the structural transitions, such as the elastic softenings and the second-order-like structural transitions, observed in both V_3Si and Nb_3Sn. Earlier works on A15 compounds were reviewed by Weger and Goldberg [5] and Izyumov and Kurmaev [6]. In a later theory on A15 compounds, Yu and Anderson [7] proposed a local-phonon model, in which double-well potentials for atoms result from strong interactions between atoms and itinerant electrons. In the present paper, we concentrate our attention on the Γ_{12} subband model as a prototype of the BJT effect model.

Much more recently, martensitic transitions in some ferromagnetic shape-memory alloys with Heusler-type structures have been attracting the attention of researchers [8,9]. Many of them are considering that the appearances of those martensitic transitions can be ascribed to the BJT effect [10–14]. In addition, the appearance of structural transitions in vanadium under high pressures was attributed to the BJT effect [15]. In fact, electronic band calculations showed that the total energies of these distorted metals are lower than those of the undistorted ones. Nevertheless, it seems that the question as to whether the BJT effect works on these metals still remains to be answered from both experimental and theoretical points of view.

In the past, extensive experimental and theoretical studies on the JT effect have already been performed, which were summed up by Kaplan and Vekhter [16] and Bersuker [17]. In this paper, we aim to clarify an aspect of BJT metals, i.e., an effect of an external pressure on band electrons pertaining to the BJT effect. We consider the case where a local pressure, i.e., a space-dependent pressure at the position x, $\delta P(x)$, induces a local distortion $\delta u(x)$. The induced distortion $\delta u(x)$ changes locally the energy of BJT electrons and causes flowing of the BJT electrons in space. These considerations inspire us to investigate an electromotive power generated by pressures with their gradients, i.e., pressure-gradient electromotive power.

Generally speaking, band electrons in usual metals with no BJT effect can be moved, more or less, by producing local distortions which have the same symmetry of the bulk crystal. Such local distortions can change locally the band electronic states and force electrons to flow into low-energy states. However, the BJT metals are expected to behave

*kataokam@kxe.biglobe.ne.jp

differently from the usual metals, because in the BJT metals, BJT distortions have symmetries different from those of original bulk crystals and couple differently to electrons in different BJT electronic bands. In the present paper, we will study the questions as to how each of the Γ_{12} subbands contributes to the pressure-gradient electromotive power and how the structural instability affects this power. Especially, we will be interested in the effect of the elastic softening resulting from the BJT structural instability on the pressure-gradient electromotive power.

In the next section, we view the equilibrium state of the BJT electron-lattice system under uniform pressures within the Γ_{12}-subband model. In Sec. III, the elastic softenings accompanied by the BJT structural transition under some uniform pressures are described. In Sec. IV, the steady state of the BJT electron system under a local pressure is derived by use of the Boltzmann equation. In Sec. V, the obtained steady state is shown to give the pressure-gradient electromotive power. In Sec. VI, a measurement system for the pressure-gradient electromotive power is proposed. Finally (in Sec. VII), summary and concluding remarks are given.

II. EQUILIBRIUM ELECTRON-LATTICE SYSTEM UNDER UNIFORM PRESSURES

The electronic band calculations on some A15 compounds with the cubic structure already showed that Γ_{12} doublet states Ψ_2 and Ψ_3 appear at the Γ point and two electronic bands evolve from the Γ_{12} states near the Fermi level ϵ_F [2]. The two bands, say the Γ_{12} subbands, are very flat and almost degenerate around ϵ_F. Assuming that the Γ_{12} subbands are responsible for the structural transition in A15 compounds, we pay attention to the two Γ_{12} subbands centered at the Γ point in the $\mathbf{k}$ space. The two bands can couple to bulk distortions, i.e., an orthorhombic distortion u_2 and a tetragonal distortion u_3, which are defined by

$$u_2 = (e_{xx} - e_{yy})/\sqrt{2} \text{ and } u_3 = (2e_{zz} - e_{xx} - e_{yy})/\sqrt{6}, \quad (1)$$

where e_{ii} ($i = x,\ y,$ and z) are the strain components. Moreover, the A15-type structure has internal ionic displacement (optic) modes Q_2 and Q_3, which have the same symmetry as those of u_2 and u_3, respectively. Although the Γ_{12} subbands can also couple to Q_2 and Q_3 [4], effects of Q_2 and Q_3 are neglected in the present paper because these optic modes do not change the qualitative nature of the structural transition.

After the $\mathbf{k}\cdot\mathbf{p}$ perturbation theory [4,18] is applied to the two Γ_{12} subbands in the presence of the bulk distortions u_2 and u_3, the effective Hamiltonian of the total electron-lattice system with crystal volume V is found to be approximately expressed as follows [3,4]:

$$H = \frac{1}{2}Vc_0u^2 + VP_3u_3 + \sum_{\nu=2,3}\sum_{\mathbf{k},\sigma}\epsilon_{\mathbf{k},\nu}a^\dagger_{\mathbf{k},\nu,\sigma}a_{\mathbf{k},\nu,\sigma}, \quad (2)$$

$$\epsilon_{\mathbf{k},\nu} = \epsilon_{\mathbf{k}} + (-1)^\nu\sqrt{c_0v_c}g_0u, \quad \left(\epsilon_{\mathbf{k}} = \frac{\hbar^2k^2}{2m^*}\right), \quad (3)$$

$$u = \sqrt{u_2^2 + u_3^2}. \quad (4)$$

The first term in Eq. (2) is the elastic energy in the presence of bulk distortions u_2 and u_3. The elastic constant $c_0 = c^0_{11} - c^0_{12}$ is defined to be the one in the absence of the BJT effect. The second term is the energy change by application of an external uniform stress P_3 to affect only u_3. For convenience, the stresses P_3 are always called pressures by defining that a positive or negative P_3 corresponds to a compressive or tensile stress, respectively. See Appendix A for relations between uniaxial pressures P_i ($i = x,\ y,$ and z) and the pressures for normal modes of bulk distortion.

The third term in Eq. (2) is the energy of electrons in the Γ_{12} subbands, which consist of two bands labeled $\nu = 2$ and $\nu = 3$. $a^\dagger_{\mathbf{k},\nu,\sigma}$ and $a_{\mathbf{k},\nu,\sigma}$ are the creation and annihilation operators, respectively, of the electron with wave vector $\mathbf{k}$ and spin $\sigma = \uparrow$ or $\downarrow$ in the ν band. Its one-electron energy $\epsilon_{\mathbf{k},\nu}$ is given by Eq. (3). As seen in Eq. (3), the two Γ_{12} subbands have the same effective mass m^*. The expression of $\epsilon_{\mathbf{k},\nu}$, Eq. (3), includes the BJT-coupling term, $(-1)^\nu\sqrt{c_0v_c}g_0u$, in which v_c is the volume of a unit cell and $g_0(>0)$ is the constant of the BJT coupling between the band electrons and the bulk distortions. The nonvanishing BJT-coupling term splits the two degenerate bands. The lower and upper bands are named $\nu = 3$ and $\nu = 2$, respectively, irrespective of the signs of u_2 and u_3.

The BJT coupling in Eq. (3) is isotropic in the $u_2 - u_3$ plane because of the symmetry of the Γ_{12} states. Anisotropic natures of H (except for the P_3 term) in the $u_2 - u_3$ plane should originate from some higher order terms of u_2 and u_3, which are not included in Eq. (2). One of such term is the anharmonic elastic energy, whose effect on the structural transition will be described in Appendix B. Putting this anharmonic elastic energy together with the pressure term in Eq. (2) in mind, we consider tetragonal structures with $u_3 \neq 0$ and $u_2 = 0$ for equilibrium ones.

The free energy of the Γ_{12} subband electrons-distortion system with a tetragonal structure under a pressure P_3 can be derived by use of Eqs. (2)–(4) as follows:

$$F/V = \frac{1}{2}c_0u_3^2 + P_3u_3 + \mu n - k_BT\sum_{\nu=2,3}\int_0^\infty D(\epsilon) \times \ln\left\{1 + \exp\left[-\left(\frac{\epsilon + (-1)^\nu\sqrt{c_0v_c}g_0|u_3| - \mu}{k_BT}\right)\right]\right\}d\epsilon, \quad (5)$$

$$D(\epsilon) = \frac{1}{2\pi^2}\left(\frac{2m^*}{\hbar^2}\right)^{3/2}\sqrt{\epsilon}, \quad (6)$$

where $D(\epsilon)$ is the density of states with spin degeneracy per unit volume for each Γ_{12} subband at energy ϵ which is measured from the bottom of the degenerate Γ_{12} subbands in the cubic phase, T is temperature, μ is the chemical potential, and n is the total electron number in the Γ_{12} subbands in unit volume.

In Eq. (5), it has already been assumed that a total electron number n in the Γ_{12} subbands is independent of the distortions u_2 and u_3. In real crystals, however, Γ_{12} subbands usually overlap with other bands near the Fermi level. Therefore, a splitting of the Γ_{12} subbands by distortions causes redistributions of electrons between the Γ_{12} subbands and others, and then n depends on the distortion. Nevertheless, we proceed with the study on the BJT effect under the constant n by taking into account the following: (1) When the band splitting is

small enough to allow both bands to be partially occupied by electrons, an increase and decrease in the electron numbers of the bands $\nu = 3$ and 2, respectively, roughly cancel each other. (2) So long as the change in n by the distortions is small, various aspects of the BJT effect are expected to be unchanged.

In the equilibrium state, u_3 and μ should satisfy the conditions $(\partial F/\partial u_3) = 0$ and a constant n, which are expressed by the following equations:

$$u_3 = -\frac{P_3}{c_0} + \sqrt{\frac{v_c}{c_0}} g_0 \,\mathrm{sgn}(u_3) \int_0^\infty D(\epsilon)[f_3(\epsilon) - f_2(\epsilon)]d\epsilon, \tag{7}$$

$$n = \int_0^\infty D(\epsilon)[f_3(\epsilon) + f_2(\epsilon)]d\epsilon, \tag{8}$$

$$f_\nu(\epsilon) = \left\{1 + \exp\left[\frac{\epsilon + (-1)^\nu \sqrt{c_0 v_c} g_0 |u_3| - \mu}{k_B T}\right]\right\}^{-1}, \tag{9}$$

where $f_\nu(\epsilon)$ is the Fermi distribution function of the electron with ϵ in the ν band. In obtaining Eq. (7), we have used $|u_3| = \mathrm{sgn}(u_3)u_3$, where $\mathrm{sgn}(u_3)$ is the sign function of u_3. Note that Eq. (7) gives $\mathrm{sgn}(u_3) = -\mathrm{sgn}(P_3)$.

As already clarified in Ref. [4] and as also will be seen in the next section of the present paper, Eqs. (7)–(9) in the case of $P_3 = 0$ can show that the second-order transition from the cubic phase into the phase with the BJT distortion $u_3 \neq 0$ can appear by decreasing T and the appearance of the BJT transition is dominated by a parameter α which is defined by

$$\alpha = 2v_c D(\epsilon_F) g_0^2 = 2v_c \left(\frac{3n}{16\pi^4}\right)^{1/3} \left(\frac{2m^*}{\hbar^2}\right) g_0^2, \tag{10}$$

where ϵ_F is the Fermi energy of the undistorted crystal. The second equation in Eq. (10) has been derived by use of Eqs. (6) and (8) at absolute zero. It is noted that the BJT structural transition can occur only when $\alpha > 1$. This is because for $\alpha \leqslant 1$, a decrease of the electronic energy by the appearance of u_3 cannot overcome the increase of the elastic energy $(1/2)c_0 u_3^2$.

Figure 1 gives the calculated phase diagram in the $\alpha - T$ plane under $P_3 = 0$. This figure is derived from the fact that the elastic constant $(c_{11} - c_{12})$ at $u_3 = 0$ becomes 0 at the second-order structural transition temperature T_M and is obtained by solving Eqs. (22) and (23) in the next section. As seen in this figure, the cubic ($u_3 = 0$) and tetragonal ($u_3 \neq 0$) phases are separated by the phase boundary, on which the cubic-to-tetragonal transition occurs. When $\alpha \leqslant 1$, the cubic crystal is always stable and has degenerate bands as shown in Fig. 2(a). When $\alpha > 1$, the crystal with a nonvanishing distortion $u_3 \neq 0$ is stable below T_M. In this case, both of the two Γ_{12} subbands are partially occupied by electrons as shown in Fig. 2(b). Then, the electron-lattice system has a minimum free energy at a $u_3 \neq 0$ below T_M but the equilibrium $u_3 \neq 0$ is

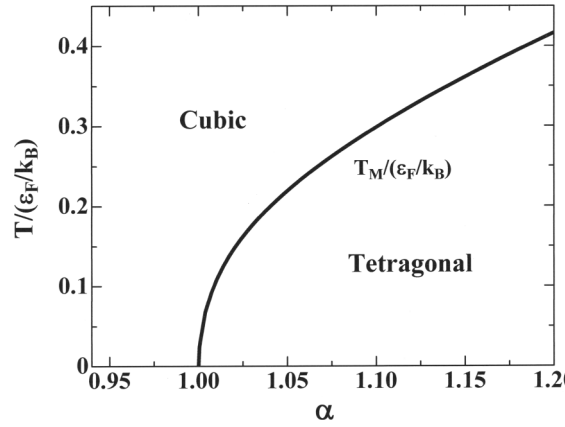

FIG. 1. Phase diagram of the equilibrium lattice structure in the α-T plane under no external pressure. α is a parameter to dominate the BJT structural transition. The cubic-to-tetragonal transition occurs at the transition temperature T_M. It is noted that the tetragonal phase does not appear when $\alpha \leqslant 1$

transitioned to $u_3 = 0$ at $T = T_M$. At absolute zero, the upper band becomes empty when α exceeds a critical value of α, α_0, which is given by

$$\alpha_0 = 3/(2^{4/3})(\sim 1.19). \tag{11}$$

Since, however, the equilibrium u_3 decreases with increasing T, the two bands $\nu = 2$ and 3 again become partially occupied, similarly to those in the case of $1 < \alpha < \alpha_0$, at temperatures except for low temperatures.

Figure 3 shows the T dependence of the equilibrium $u_3(> 0)$ which was calculated for $\alpha = 1.08$ under some fixed uniform pressures $P_3(< 0)$. Nonvanishing pressures P_3 can easily destroy the second-order transition under $P_3 = 0$ but make the BJT distortion remain even at $T > T_M$. Figure 3 holds also for the case where $u_3(< 0)$ and $P_3(> 0)$ by changing the signs of u_3 and P_3 in the figure.

When $P_3(> 0)$ is applied to a crystal with an elongation $u_3(> 0)$, or $P_3(< 0)$ is applied to a crystal with a contraction $u_3(< 0)$, those pressures P_3 with large magnitudes can convert the equilibrium distortions between $u_3 > 0$ and $u_3 < 0$. This

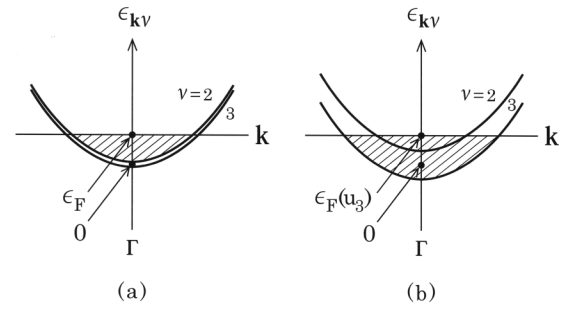

FIG. 2. Schematic diagram of the Γ_{12} subbands $\epsilon_{\mathbf{k},\nu}$ ($\nu = 2$ and 3) with the band Jahn-Teller (BJT) effect. $\mathbf{k}$ is an electron's wave vector around the Γ point. (a) Case of no BJT distortion ($\alpha \leqslant 1$). The two Γ_{12} subbands are degenerate around the Γ point and have the Fermi energy ϵ_F. (b) Case of a BJT distortion $u_3 \neq 0$. The two Γ_{12} subbands are split by $u_3 \neq 0$. When the splitting is small, both the bands are partially occupied by electrons.

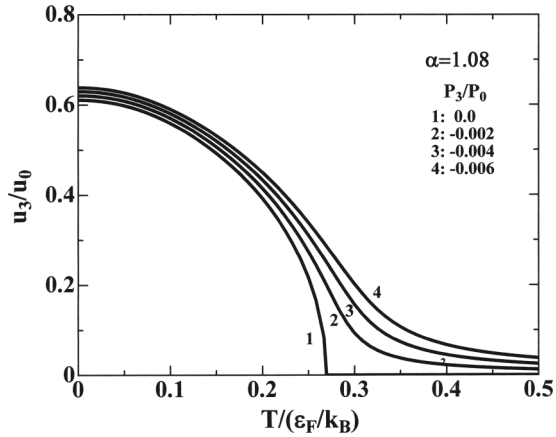

FIG. 3. Temperature dependence of the equilibrium BJT distortion $u_3(>0)$ calculated for $\alpha = 1.08$ under some uniform pressures $P_3(\leqslant 0)$. The units of u_3 and P_3 are $u_0 = \epsilon_F/(\sqrt{c_0 v_c} g_0)$ and $P_0 = \sqrt{c_0/v_c}(\epsilon_F/g_0)$, respectively. Under no uniform pressure, the second-order BJT transition occurs at the transition temperature T_M ($\sim 0.27\epsilon_F/k_B$ for $\alpha = 1.08$). This figure holds also when the signs of u_3/u_0 and P_3 are changed to be negative and positive, respectively, but with same magnitudes as those in the figure.

conversion is out of the scope of the present theory, but will be mentioned in Sec. VI in relating to measurement system for the pressure-gradient electromotive power.

III. ELASTIC CONSTANTS AFFECTED BY THE BAND JAHN-TELLER EFFECT

As will be seen in the following sections, the elastic softening plays an important role in the pressure-electric effect which is the subject of the present theory. Some characteristics of the elastic constants affected by the BJT effect were already studied before [4]. In this section, we extend this study to the case of the elastic constants under uniform pressures P_3. Also in these elastic constants, the effects of the optic modes of ionic displacement Q_2 and Q_3 are not taken into account.

Starting from an equilibrium electron-lattice system with $u_3 \neq 0$ and $u_2 = 0$ under pressure P_3, we introduce further uniform distortions δu_2 and δu_3 as well as a further uniform pressure δP_3 with small magnitudes. Then, the free energy F has the form as

$$F = F_0 + V\delta P_3 \delta u_3 + \tfrac{1}{2}V\{C_2(P_3,T)(\delta u_2)^2 + C_3(P_3,T)(\delta u_3)^2\}, \tag{12}$$

where F_0 is the free energy of the equilibrium state at $\delta u_2 = \delta u_3 = 0$ and $\delta P_3 = 0$, being obtained by substituting the solutions $u_3 \neq 0$ and $u_2 = 0$ of Eqs. (7) and (8) into Eq. (5).

In Eq. (12), $C_{2,3}(P_3, T)$ are elastic constants, which are referred to a specimen distorted tetragonally. The usual elastic constants c_{ij}, on the other hand, are defined to be referred to a cubic specimen, even when the crystal is distorted from its cubic structure. The relations between $C_{2,3}(P_3, T)$ and c_{ij} are given in Ref. [19]. Especially when $|u_3|$ is sufficiently smaller than 1, $C_2(P_3, T) \approx (c_{11} - c_{12})$ and $C_3(P_3, T) \approx (c_{33} - c_{13})$ in the tetragonal phase, while $C_2(0, T) = C_3(0, T) = (c_{11} - c_{12})$ in the cubic phase. To the following studies, $C_{2,3}(P_3, T)$ are suitably applied, rather than the elastic constants c_{ij} themselves.

To obtain $C_3(P_3, T)$ in the tetragonal phase, we substitute $(u_3 + \delta u_3)$ for u_3 in F given by Eq. (5) and expand F in powers of δu_3 up to the second-order term $(\delta u_3)^2$. After the expanded F is compared with the one given by Eq. (12), we have

$$C_3(P_3,T) = c_0 - \frac{1}{k_B T}\left\{\left[\sqrt{c_0 v_c}\, g_0\ \mathrm{sgn}(u_3) - \left(\frac{\partial\mu}{\partial u_3}\right)_0\right]^2 W_2(P_3,T) + \left[\sqrt{c_0 v_c}\, g_0\ \mathrm{sgn}(u_3) + \left(\frac{\partial\mu}{\partial u_3}\right)_0\right]^2 W_3(P_3,T)\right\}, \tag{13}$$

with

$$W_\nu(P_3,T) = \int_0^\infty D(\epsilon) f_\nu(\epsilon)(1 - f_\nu(\epsilon))d\epsilon, \ (\nu = 2 \text{ or } 3), \tag{14}$$

where $(\partial\mu/\partial u_3)_0$ and $W_\nu(P_3, T)$ are their quantities at $\delta u_2 = \delta u_3 = 0$ and $\delta P_3 = 0$. Noting that μ is an implicit function of u_3 through Eqs. (8) and (9), we differentiate both sides of Eq. (8) with respect to u_3 to obtain

$$\left(\frac{\partial\mu}{\partial u_3}\right)_0 = \sqrt{c_0 v_c}\, g_0\ \mathrm{sgn}(u_3)\left[\frac{W_2(P_3,T) - W_3(P_3,T)}{W_2(P_3,T) + W_3(P_3,T)}\right]. \tag{15}$$

Substitution of Eq. (15) into Eq. (13) gives

$$C_3(P_3,T) = c_0[1 - \alpha X(P_3,T)], \tag{16}$$

where $X(P_3, T)$ has been defined by

$$X(P_3,T)^{-1} = \tfrac{1}{2}k_B T D(\epsilon_F)[W_2(P_3,T)^{-1} + W_3(P_3,T)^{-1}], \tag{17}$$

and α was already presented in Eq. (10). $C_3(P_3, T)$ given by Eq. (16) does not depend on the sign of P_3.

The obtained $C_3(P_3, T)$ expressed by Eq. (16) can be used to know the equilibrium distortion δu_3 induced by δP_3. Minimizing F given by Eq. (12) with respect to δu_3, we get

$$\frac{\delta u_3}{\delta P_3} = -\frac{1}{C_3(P_3,T)}. \tag{18}$$

Similar calculations on $C_2(P_3, T)$ to the above show that $C_2(P_3, T)$ is also strongly affected by the BJT structural transition. However, we do not go into the details of $C_2(P_3, T)$, which is not used in the following arguments.

On the other hand, the elastic constant in the cubic phase above T_M under no pressure, $C_3(0, T)$, is known by use of Eqs. (16), (17), and (14) at $u_3 = 0$ as follows:

$$C_3(0,T)(= c_{11} - c_{12}) = c_0[1 - \frac{\alpha}{k_B T D(\epsilon_F)}\int_0^\infty D(\epsilon) f(\epsilon,T)(1 - f(\epsilon,T))d\epsilon], \tag{19}$$

where $f(\epsilon, T)$ is defined by

$$f(\epsilon,T) = \{1 + \exp[(\epsilon - \mu)/k_B T)]\}^{-1}, \tag{20}$$

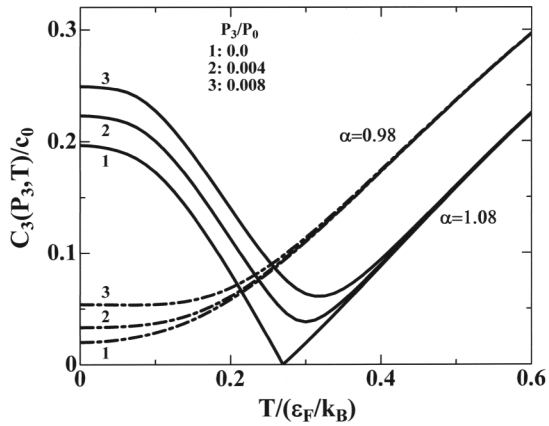

FIG. 4. Temperature dependence of the elastic constant $C_3(P_3, T)$ calculated in the equilibrium state with $u_3(< 0)$ under some uniform pressures $P_3(> 0)$. The unit of P_3 is $P_0 = \sqrt{c_0/v_c}(\epsilon_F/g_0)$. The solid lines were calculated for $\alpha = 1.08$, which gives $T_M \sim 0.27\epsilon_F/k_B$. It is noted that softenings of $C_3(P_3, T)$ appear at temperatures near T_M but remain even at low temperatures. The dot-dash lines were calculated for $\alpha = 0.98$, which does not make appearance of the BJT transition. This figure holds also when the signs of P_3 in the figure are changed to be negative without changing their magnitudes.

with μ satisfying

$$n = 2\int_0^\infty D(\epsilon) f(\epsilon, T) d\epsilon. \tag{21}$$

At the second-order-transition temperature $T = T_M$, the above $C_3(0, T)$ should become 0, so T_M is obtained by solving numerically the simultaneous equations for T_M and μ as follows:

$$\frac{\alpha}{D(\epsilon_F)}\int_0^\infty D(\epsilon) f(\epsilon, T_M))[1 - f(\epsilon, T_M)] d\epsilon = k_B T_M, \tag{22}$$

$$n = 2\int_0^\infty D(\epsilon) f(\epsilon, T_M) d\epsilon. \tag{23}$$

The obtained T_M was already shown as a function of α in Fig. 1.

Figure 4 shows the elastic constant $C_3(P_3, T)$ calculated under some uniform pressures P_3 in the two cases of $1 < \alpha < \alpha_0$ and $\alpha \leqslant 1$. As seen in this figure, the elastic constant $C_3(P_3, T)$ for $\alpha = 1.08$ is drastically softened in a wide region of temperature. Especially at $T = T_M$, $C_3(0, T)$ vanishes because of the BJT structural transition. The softenings remain even at low temperatures, because the electronic and lattice contributions to $C_3(P_3, T)$ partially cancel each other. These softenings are hardly recovered by the presence of nonvanishing pressures P_3.

When $\alpha \leqslant 1$, the BJT structural transition does not occur. Figure 4 also shows $C_3(P_3, T)$ calculated for $\alpha = 0.98$ under some uniform pressures. As seen in this figure, $C_3(P_3, T)$ is again considerably softened in a wide region of temperature but especially at low temperatures. This is because the lattice and electronic contributions to the elastic constants largely cancel each other, although the latter can not overcome the former.

In the case of $\alpha_0 < \alpha$, $C_3(P_3, T)$ recovers to c_0 at absolute zero without exhibiting its elastic softening [4]. Nevertheless, $C_3(P_3, T)$ is again considerably softened in a wide region of temperature except for low temperatures because the equilibrium u_3 is decreased with increasing temperature.

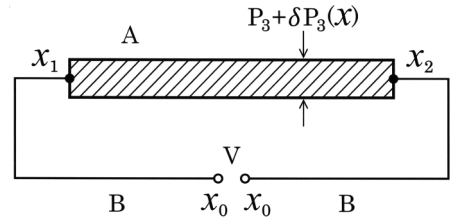

FIG. 5. Circuit to observe the pressure-gradient electromotive power $A(P_3, T)$. The sample A is a BJT metal which spreads along the x axis from $x = x_1$ to $x = x_2$ under no pressure. The wire B is a usual metal with no BJT effect. The sample A is subjected to a uniform pressure P_3 and a local pressure $\delta P_3(x)$. A voltmeter is set at the position $x = x_0$.

At the end of this section, we note the kind of structural phase transitions obtained for A15 compounds. The Γ_{12} subband model gives the second-order structural transition, which is attributed to the double degeneracy of the Γ_{12} subbands. In fact, some A15 compounds exhibit structural transitions close to those of second order [20,21]. In general, however. real crystals have the anharmonic elastic energy proportional to u_3^3, which was not included in Eq. (2). As will be summarized in Appendix B, the u_3^3 term changes the BJT structural transition to be of first order and modifies the elastic constant $C_3(0, T)$. As a result, $C_3(0, T)$ does not vanish at any temperature even under no pressure. It is noted that the second-order-like cubic-to-tetragonal transitions in A15 compounds suggest weak effects of the anharmonic energy in these compounds.

IV. STEADY ELECTRON SYSTEM UNDER A PRESSURE GRADIENT

Hereafter, we consider a sample of a BJT metal, whose shape has a sufficiently long length along the x axis as illustrated in Fig. 5. It is assumed that a local (i.e., space-dependent) pressure at position x, $\delta P_3(x)$, is applied to this sample additionally to the uniform pressure P_3. The total pressure $P_{3,\mathrm{tot}}(x)$ at x is expressed by

$$P_{3,\mathrm{tot}}(x) = P_3 + \delta P_3(x). \tag{24}$$

P_3 affects the equilibrium BJT distortion u_3 as shown in Sec. II, but $\delta P_3(x)$ induces a local (i.e., space-dependent) distortion $\delta u_3(x)$ additional to u_3. As a result, the total distortion at x, $u_{3,\mathrm{tot}}(x)$, becomes

$$u_{3,\mathrm{tot}}(x) = u_3 + \delta u_3(x). \tag{25}$$

In the following, it is required that $\delta P_3(x)$ and $\delta u_3(x)$ are almost constant on a microscopic scale, e.g., a lattice constant, but they vary slowly with x on a macroscopic scale, e.g., a dimension of the sample [22]. In a region containing x, therefore, the electron-lattice system is considered to be in a local equilibrium state, where the distribution function of the

electron in the $(\mathbf{k}, \nu)$ state can be expressed by

$$f_\nu^0(\epsilon_\mathbf{k}, x) = \left\{1 + \exp\left[\frac{\epsilon_\mathbf{k} + (-1)^\nu \sqrt{c_0 v_c} g_0 |u_{3,\mathrm{tot}}(x)| - \mu(x)}{k_\mathrm{B} T}\right]\right\}^{-1}. \tag{26}$$

When the electron system is not equilibrium by some reason, electrons flow toward the equilibrium state. Then, the distribution function of the $(\mathbf{k}, \nu)$ electron around x, $f_\nu(\epsilon_\mathbf{k}, x)$, depends on time t. According to the Boltzmann theory [22,23], $(\partial f_\nu(\epsilon_\mathbf{k}, x)/\partial t)$ arises from diffusions of the electron in the phase space and scatterings of the electron by various causes. After experiencing the diffusions and scatterings of electrons, the electron system falls into a steady state with $(\partial f_\nu(\epsilon_\mathbf{k}, x)/\partial t) = 0$. In this steady state, $(\partial f_\nu(\epsilon_\mathbf{k}, x)/\partial t)$ caused by electron scatterings, $(\partial f_\nu(\epsilon_\mathbf{k}, x)/\partial t)_\mathrm{s}$, should satisfy the Boltzmann equation as follows:

$$\begin{aligned}\left(\frac{\partial f_\nu(\epsilon_\mathbf{k}, x)}{\partial t}\right)_\mathrm{s} = \Bigg[& v_{\mathbf{k},x}\left(\frac{\partial \mu}{\partial x}\right)\left(\frac{\partial}{\partial \mu}\right) \\ & + v_{\mathbf{k},x}\left(\frac{\partial \delta P_3(x)}{\partial x}\right)\left(\frac{\partial \delta u_3(x)}{\partial \delta P_3(x)}\right)\left(\frac{\partial}{\partial \delta u_3(x)}\right) \\ & + \frac{eE_x}{\hbar}\left(\frac{\partial}{\partial k_x}\right)\Bigg] f_\nu^0(\epsilon_\mathbf{k}, x),\end{aligned} \tag{27}$$

where E_x is an electric field along the x axis, $v_{\mathbf{k},x}$ is the x component of the velocity of the electron with the energy $\epsilon_{\mathbf{k},\nu}$, and $e(<0)$ is the electric charge.

The scattering term $(\partial f_\nu(\epsilon_\mathbf{k}, x)/\partial t)_\mathrm{s}$ on the left-hand side of Eq. (27) depends on transition probabilities between different electronic states. Here, the probability of an electronic transition from a $(\mathbf{k}, \nu)$ state into another $(\mathbf{k}', \nu')$ state is denoted by $w(\mathbf{k}, \nu \to \mathbf{k}', \nu')$. Then, the change in $f_\nu(\epsilon_\mathbf{k}, x)$ by electron scatterings is written as

$$\sum_{\mathbf{k}', \nu'} [w(\mathbf{k}', \nu' \to \mathbf{k}, \nu) - w(\mathbf{k}, \nu \to \mathbf{k}', \nu')]. \tag{28}$$

The various transition probabilities $w(\mathbf{k}, \nu \to \mathbf{k}', \nu')$ affect each other through the distribution functions $f_\nu(\epsilon_\mathbf{k}, x)$. After those electron scatterings are done self-consistently in a steady state, each $f_\nu(\epsilon_\mathbf{k}, x)$ has its own time dependence. In the steady state, we employ the relaxation-time approximation as follows:

$$\left(\frac{\partial f_\nu(\epsilon_\mathbf{k}, x)}{\partial t}\right)_\mathrm{s} = -\frac{\Delta f_\nu(\epsilon_\mathbf{k}, x)}{\tau_\nu(\epsilon_\mathbf{k})}, \tag{29}$$

$$\Delta f_\nu(\epsilon_\mathbf{k}, x) = f_\nu(\epsilon_\mathbf{k}, x) - f_\nu^0(\epsilon_\mathbf{k}, x), \tag{30}$$

where $\tau_\nu(\epsilon_\mathbf{k})$ is a phenomenologically-introduced relaxation time of the electron in the $(\mathbf{k}, \nu)$ state. Equations (27), (29), and (30) give

$$\begin{aligned}\Delta f_\nu(\epsilon_\mathbf{k}, x) = & \left(\frac{\partial f_\nu(\epsilon_\mathbf{k})}{\partial \epsilon_\mathbf{k}}\right)\tau_\nu(\epsilon_\mathbf{k}) v_{\mathbf{k},x} \\ & \times \Bigg[-eE_x + \frac{\partial \mu}{\partial x} \\ & + (-1)^\nu \mathrm{sgn}(u_{3,\mathrm{tot}}(x))\left(\frac{\sqrt{c_0 v_c} g_0}{C_3(P_3, T)}\right)\left(\frac{\partial \delta P_3(x)}{\partial x}\right)\Bigg],\end{aligned} \tag{31}$$

where $(\partial f_\nu^0(\epsilon_\mathbf{k}, x))/\partial \epsilon_\mathbf{k})$ has been approximated to be $(\partial f_\nu(\epsilon_\mathbf{k})/\partial \epsilon_\mathbf{k})$ and the next relation has been used:

$$\left(\frac{\partial \delta u_3(x)}{\partial \delta P_3(x)}\right) = \left(\frac{\partial \delta u_3}{\partial \delta P_3}\right) = -\frac{1}{C_3(P_3, T)}. \tag{32}$$

In Eq. (31), it should be noted that the pressure gradient $(\partial \delta P_3(x)/\partial x)$ contributes to $\Delta f_\nu(\epsilon_\mathbf{k}, x)$. This originates from the fact that $\delta P_3(x)$ produces $\delta u_3(x)$, which changes locally energies of the Γ_{12} subbands electrons.

Even in the band structure of BJT metals, the Fermi level ϵ_F also crosses some electronic bands other than the Γ_{12} subbands, say ξ bands. The ξ bands around the Γ point do not couple linearly to u_2 and u_3. As stated in Sec. II, the electron redistribution between the ξ and ν bands is considered to be small enough to be neglected in the case of small splittings of the two Γ_{12} subbands. This situation corresponds to an approximation that electrons both in the Γ_{12} and ξ bands have a common chemical potential μ determined by Eq. (8). Then, the deviation of the distribution function of the ξ electrons, $\Delta f_\xi(\epsilon_\mathbf{k})$, is expressed as

$$\Delta f_\xi(\epsilon_\mathbf{k}, x) = \left(\frac{\partial f_\xi(\epsilon_\mathbf{k})}{\partial \epsilon_\mathbf{k}}\right)\tau_\xi(\epsilon_\mathbf{k}) v_{\mathbf{k},x}\left[-eE_x + \frac{\partial \mu}{\partial x}\right], \tag{33}$$

where $\tau_\xi(\epsilon_\mathbf{k})$ and $v_{\mathbf{k},x}$ are the relaxation time and the velocity (along the x direction) of the electron with $\mathbf{k}$ in the ξ band. On the right-hand side of Eq. (33), the term $(\partial \delta P_3(x)/\partial x)$ does not appear because the ξ bands do not couple linearly to δu_3.

Once the deviations of the distribution functions are obtained, the total electric current along the x direction, J_x, can be given by

$$\begin{aligned}J_x &= 2e\left\{\sum_{\mathbf{k},\nu} v_{\mathbf{k},x}\Delta f_\nu(\epsilon_\mathbf{k}) + \sum_{\mathbf{k},\xi} v_{\mathbf{k},x}\Delta f_\xi(\epsilon_\mathbf{k})\right\} \\ &= 2e\sum_{\mathbf{k},\nu}\left(\frac{\partial f_\nu(\epsilon_\mathbf{k})}{\partial \epsilon_\mathbf{k}}\right)\tau_\nu(\epsilon_\mathbf{k}) v_{\mathbf{k},x} v_{\mathbf{k},x}\Bigg[-eE_x + \frac{\partial \mu}{\partial x} \\ &\qquad + (-1)^\nu \mathrm{sgn}(u_{3,\mathrm{tot}}(x))\left(\frac{\sqrt{c_0 v_c} g_0}{C_3(P_3, T)}\right)\left(\frac{\partial \delta P_3(x)}{\partial x}\right)\Bigg] \\ &\quad + 2e\sum_{\mathbf{k},\xi}\left(\frac{\partial f_\xi(\epsilon_\mathbf{k})}{\partial \epsilon_\mathbf{k}}\right)\tau_\xi(\epsilon_\mathbf{k}) v_{\mathbf{k},x} v_{\mathbf{k},x}\left[-eE_x + \frac{\partial \mu}{\partial x}\right].\end{aligned} \tag{34}$$

When $J_x = 0$, therefore, the electric field along the x direction at the position x, $E_x(g_0, x)$, should become

$$\begin{aligned}E_x(g_0, x) = \frac{1}{e}\Bigg\{ & \frac{\partial \mu}{\partial x} + \mathrm{sgn}(u_{3,\mathrm{tot}}(x))\left(\frac{\sqrt{c_0 v_c} g_0}{C_3(P_3, T)}\right) \\ & \times \left[\frac{L_2(P_3, T) - L_3(P_3, T)}{L_2(P_3, T) + L_3(P_3, T) + \sum_\xi L_\xi(T)}\right] \\ & \times \left(\frac{\partial \delta P_3(x)}{\partial x}\right)\Bigg\},\end{aligned} \tag{35}$$

with

$$L_\nu(P_3,T)=\frac{2}{3}\frac{e^2}{m^*}\int_0^\infty\left(-\frac{\partial f_\nu(\epsilon)}{\partial\epsilon}\right)\tau_\nu(\epsilon)\epsilon D(\epsilon)d\epsilon, \quad (36)$$

$$L_\xi(T)=\frac{2}{3}\frac{e^2}{m_\xi^*}\int_{-\infty}^\infty\left(-\frac{\partial f_\xi(\epsilon)}{\partial\epsilon}\right)\tau_\xi(\epsilon)\epsilon D_\xi(\epsilon)d\epsilon, \quad (37)$$

where m_ξ^* is the effective mass of the ξ band.

V. ELECTROMOTIVE POWER GENERATED BY A PRESSURE GRADIENT

Let us derive the electromotive power originating from $E_x(g_0,x)$ given by Eq. (35). To do this, we consider the electric circuit shown in Fig. 5. In this figure, sample A is the BJT metal with the electric field $E_x(g_0,x)$ but wire B is a usual metal with $E_x(0,x)=(1/e)(\partial\mu/\partial x)$. Sample A is subjected to the pressure $P_{3,\mathrm{tot}}(x)=P_3+\delta P_3(x)$, where P_3 produces or enhances u_3 and $\delta P_3(x)$ produces $\delta u_3(x)$. Then, the difference in the electric potential ϕ, $\Delta\phi$, at x_0 is given by

$$\begin{aligned}\Delta\phi&=-\int_{x_0}^{x_1}E_x(0,x)dx-\int_{x_1}^{x_2}E_x(g_0,x)dx\\&\quad-\int_{x_2}^{x_0}E_x(0,x)dx\\&=-\mathrm{sgn}(u_{3,\mathrm{tot}}(x))\frac{1}{e}\left(\frac{\sqrt{c_0v_c}g_0}{C_3(P_3,T)}\right)\\&\quad\times\left[\frac{L_2(P_3,T)-L_3(P_3,T)}{L_2(P_3,T)+L_3(P_3,T)+\sum_\xi L_\xi(T)}\right]\\&\quad\times[\delta P_3(x_2)-\delta P_3(x_1)],\end{aligned} \quad (38)$$

where $\oint(\partial\mu/\partial x)dx=0$ has been already taken into account. This means that the electric field at x along the x direction, $E_x(x)$, in sample A is given by

$$E_x(x)=A(P_3,T)\left(\frac{\partial|\delta P_3(x)|}{\partial x}\right), \quad (39)$$

$$\begin{aligned}A(P_3,T)&=\mathrm{sgn}(u_{3,\mathrm{tot}}(x))\mathrm{sgn}(\delta P_3(x))\\&\quad\times A_0\left(\frac{c_0}{C_3(P_3,T)}\right)\left[\frac{L_2(P_3,T)-L_3(P_3,T)}{L_2(P_3,T)+L_3P_3,T)}\right],\end{aligned} \quad (40)$$

where

$$A_0=\frac{1}{e\lambda}\sqrt{\frac{v_c}{c_0}}g_0\ (<0), \quad (41)$$

with

$$\lambda=1+\frac{\sum_\xi L_\xi(T)}{L_2(P_3,T)+L_3(P_3,T)}. \quad (42)$$

Especially, when P_3 and $\delta P_3(x)$ are additive to each other, i.e., $\mathrm{sgn}(P_3)=\mathrm{sgn}(\delta P_3(x))$, the equilibrium conditions for u_3 and $\delta u_3(x)$, Eqs. (7) and (18), give

$$\begin{aligned}&\mathrm{sgn}(u_3)=-\mathrm{sgn}(P_3),\ \ \mathrm{sgn}(\delta u_3(x))=-\mathrm{sgn}(\delta P_3(x)),\\&\text{and }\mathrm{sgn}(u_{3,\mathrm{tot}}(x))=-\mathrm{sgn}(\delta P_3(x)).\end{aligned} \quad (43)$$

Then, Eq. (40) is simplified to become as follows:

$$A(P_3,T)=A_0\left(\frac{c_0}{C_3(P_3,T)}\right)\left[\frac{L_3(P_3,T)-L_2(P_3,T)}{L_3(P_3,T)+L_2P_3,T)}\right], \quad (44)$$

A_0 being same as the one given by Eq. (41). It is noted that $A(P_3,T)$ given by Eq. (44) does not depend on the sign of P_3. This is because the band structure consisting of the bands $\nu=2$ and $\nu=3$ split by the BJT coupling is independent of the sign of u_3 in Eq. (3).

Equation (39) shows that the pressure gradient generates the electric field $E_x(x)$ in the BJT metal and the magnitude of the generated electromotive power is represented by the coefficient $A(P_3,T)$ defined by Eqs. (40) and (44). In the present paper, we call $A(P_3,T)$ the pressure-gradient electromotive power.

The pressure-gradient electric effect derived here can be compared with the well-established piezoelectric effect. The latter originates from the fact that electric dipoles of ionic pairs in dielectric crystals with no inversion center are not canceled under uniform pressures. The former, on the other hand, originates from flows of conducting electrons in metals under pressures with their gradients. This situation is parallel rather to that of the thermoelectric effect, which appears in metals under temperature gradients.

From Eqs. (40) and (44), the following properties of $A(P_3,T)$ are derived. When $u_3=0$ at $T>T_\mathrm{M}$ under $P_3=0$, $L_2(0,T)=L_3(0,T)$ and therefore $A(0,T)=0$. This is because the contributions of the two bands $\nu=2$ and 3 cancel each other in spite of their nonvanishing values in the cubic phase. In BJT metals with $\alpha\leqslant 1$, any spontaneous equilibrium distortion does not appear in the absence of P_3. However, a nonvanishing P_3 produces u_3 to give $A(P_3,T)\neq 0$. Another important property of $A(P_3,T)$ given by Eqs. (40) and (44) is that $A(P_3,T)$ is considerably enhanced by the elastic softening in $C_3(P_3,T)$. This enhancement appears by the following reason: When $C_3(P_3,T)$ is softened by the BJT effect, a weak pressure gradient $(\partial\delta P_3(x)/\partial x)$ can induce a large distortion gradient $(\partial\delta u_3(x)/\partial x)$, as seen from the relation

$$\left(\frac{\partial\delta u_3(x)}{\partial x}\right)=-\frac{1}{C_3(P_3,T)}\left(\frac{\partial\delta P_3(x)}{\partial x}\right). \quad (45)$$

Through u_3 and $C_3(P_3,T)$ in $A(P_3,T)$, $A(P_3,T)$ exhibits its strong P_3 and T dependencies.

The quantity $[L_2(P_3,T)+L_3(P_3,T)]$ in Eq. (42) is shown to be independent of the splitting of the Γ_{12} subbands and $\sum_\xi L_\xi(T)$ is expected to depend hardly on T around T_M. As a result, λ can be almost constant. Through Eq. (36), $A(P_3,T)$ given by Eqs. (40) and (44) depends on the relaxation times $\tau_\nu(\epsilon)$. When, however, both $\tau_2(\epsilon)$ and $\tau_3(\epsilon)$ are approximated to be $\tau(\mu)$ in Eq. (36), $\tau(\mu)$ is reducible in Eqs. (40) and (44), being eliminated from $A(P_3,T)$.

In the above, the case of the local pressure $\delta P_3(x)$ additional to the uniform pressure P_3 has been considered. We mention another case where a local pressure $\delta P_2(x)$ to produce $\delta u_2(x)$ is applied instead of $\delta P_3(x)$. Since $u_3\neq 0$ and $u_2=0$ remain in the equilibrium state, we have

$$\begin{aligned}\frac{\partial}{\partial x}\sqrt{(\delta u_2(x))^2+u_3^2}&=\frac{\partial\delta u_2(x)}{\partial x}\left[\frac{\delta u_2(x)}{\sqrt{(\delta u_2(x))^2+u_3^2}}\right]_{\delta u_2(x)=0}\\&=0.\end{aligned} \quad (46)$$

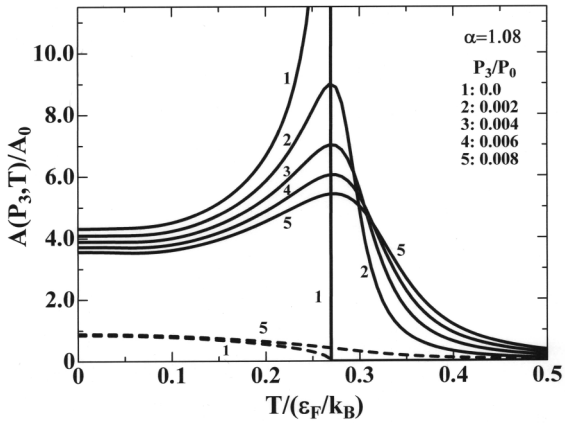

FIG. 6. Pressure-gradient electromotive power $A(P_3, T)$ calculated for $\alpha = 1.08$ as a function of temperature T under some uniform pressures P_3. The calculation was made by use of Eq. (44). The unit of $A(P_3, T)$ is $A_0(< 0)$ given by Eq. (41), while the unit of P_3 is $P_0 = \sqrt{c_0/v_c}(\epsilon_F/g_0)$. The solid lines are $A(P_3, T)$ in the metal subjected to the elastic softening by the BJT effect. In the case of $P_3 = 0$, $A(0, T)$ vanishes above T_M ($\sim 0.27\epsilon_F/k_B$ for $\alpha = 1.08$). For comparison, the broken lines show $A(P_3, T)$ calculated by assuming $[c_0/C_3(P_3, T))] = 1$, which excludes an enhancement of $A(P_3, T)$ by the elastic softening. This figure holds also when the signs of P_3 in the figure are changed to be negative but with same magnitudes as those in the figure.

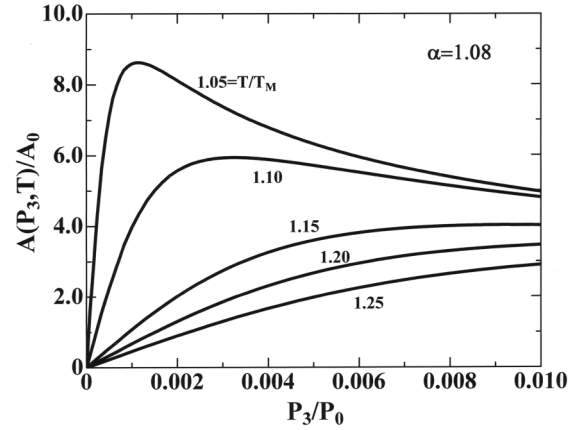

FIG. 7. Pressure-gradient electromotive power $A(P_3, T)$ calculated for $\alpha = 1.08$ as a function of the uniform pressure P_3. The calculations were made by use of Eq. (44) at some temperatures T above T_M ($\sim 0.27\epsilon_F/k_B$ for $\alpha = 1.08$). The unit of $A(P_3, T)$ is $A_0(< 0)$ given by Eq. (41), while the unit of P_3 is $P_0 = \sqrt{c_0/v_c}(\epsilon_F/g_0)$. This figure holds also when the positive values of P_3/P_0 in the abscissa are changed to be negative but with same magnitudes as those in the abscissa.

This proves that a pressure gradient $(\partial\delta P_2(x)/\partial x)$ cannot generate any electromotive power in the equilibrium state with $u_3 \neq 0$ and $u_2 = 0$.

Figure 6 shows the calculated pressure-gradient electromotive power $A(P_3, T)$ as a function of T for $\alpha = 1.08$ under some fixed compressive stresses $P_3(> 0)$. This calculation was made by use of Eq. (44). As shown by the solid lines in this figure, $A(P_3, T)$ becomes nonvanishing in a wide region of temperature. When $P_3 = 0$, $A(P_3, T)$ becomes nonvanishing only below T_M, because the spontaneous u_3 makes $L_2(0, T) \neq L_3(0, T)$. Especially at $T \to T_M - 0$ under $P_3 = 0$ in the tetragonal phase, $A(0, T)$ diverges, since $C_3(0, T) = 0$ at T_M as shown in Fig. 4. However, this divergence is arrested in real crystals, which have $C_3(P_3, T) \neq 0$ at any temperature because of the presence of the anharmonic elastic energy. (See Appendix B.) When $P_3 \neq 0$, on the other hand, $A(P_3, T)$ becomes always nonvanishing, because u_3 is induced by P_3 even above T_M. The peaks of $A(P_3, T)$ are suppressed by increasing $P_3(> 0)$. In Fig. 6, $A(P_3, T)$ which was calculated by excluding the effect of the elastic softening is also shown by the broken lines. Such calculations were made by assuming $[c_0/C_3(P_3, T)] = 1$ in Eq. (44). As seen in Fig. 6, the considerable enhancement of $A(P_3, T)$ originates from the elastic softening in $C_3(P_3, T)$. The enhancement of $A(P_3, T)$ by the elastic softening becomes always conspicuous at temperatures near T_M, so long as the BJT structural transition occurs. $A(P_3, T)$ is not changed even when the compressive stresses $P_3(> 0)$ are replaced by tensile stresses $P_3(< 0)$.

Figure 7 shows $A(P_3, T)$ calculated as a function of P_3 at some fixed temperatures above T_M. This calculation is made by use of Eq. (44). Although $A(P_3, T) = 0$ at $P_3 = 0$, a nonvanishing P_3 induces $A(P_3, T) \neq 0$, because u_3 induced by P_3 makes a difference between $L_2(P_3, T)$ and $L_3(P_3, T)$. A broad peak in the line at $T/T_M \sim 1.05$ results from the strong elastic softening in $C_3(P_3, T)$ just above T_M, which is shown in Fig. 4. Even when T is apart from T_M, the large values of $A(P_3, T)$ appear with increasing P_3 because the elastic softening continues in a wide region of T higher than T_M.

Similar calculations on $A(P_3, T)$ to those in Fig. 6 were done in a case of $\alpha \leqslant 1$, for which the BJT structural transition does not occur. In Fig. 8, $A(P_3, T)$ calculated by use of Eq. (44) for $\alpha = 0.98$ is shown by the solid lines. As seen in Fig. 8, $A(P_3, T)$ has large values at

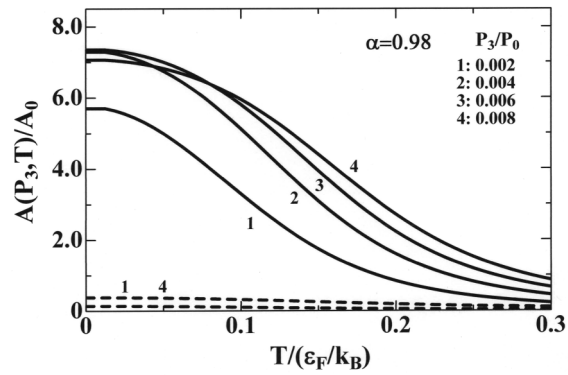

FIG. 8. Pressure-gradient electromotive power $A_3(P_3, T)$ calculated for $\alpha = 0.98$ as a function of temperature T. For this value of α, the spontaneous BJT distortion does not occur. The calculation was made by use of Eq. (44). The unit of $A(P_3, T)$ is $A_0(< 0)$ given by Eq. (41), while the unit of P_3 is $P_0 = \sqrt{c_0/v_c}(\epsilon_F/g_0)$. For comparison, the broken lines show $A(P_3, T)$ calculated by assuming $[c_0/C_3(P_3, T))] = 1$, which excludes the elastic softening. The calculations were made in the case where $P_3 > 0$. This figure holds also when the signs of P_3 in the figure are changed to be negative but with same magnitudes as those in the figure.

low temperatures when $P_3 \neq 0$. Also in Fig. 8, $A(P_3, T)$ calculated for $[c_0/C_3(P_3, T)] = 1$ with no elastic softening is shown by the broken lines. As seen in Fig. 8, $A(P_3, T)$ is again enhanced by the elastic softening in spite of no structural transition as shown in Fig. 1. This enhancement of $A(P_3, T)$ can be seen when $\alpha(\leqslant 1)$ is close to 1.

It is noted that when $\alpha_0 < \alpha$, $A(P_3, T)$ cannot be enhanced at low temperatures because $C_3(P_3, T) = c_0$ at absolute zero [4]. Also in this case, $A(P_3, T)$ is again considerably enhanced by the elastic softening at temperatures except for low temperatures, so long as the BJT structural transition occurs.

A numerical consideration on $A(P_3, T)$ of Nb_3Sn is made by use of its available data, given in Appendix C.

VI. MEASUREMENT SYSTEM FOR THE PRESSURE-GRADIENT ELECTROMOTIVE POWER

After the theory presented above, some comments are described on a possible measurement system for the pressure-gradient electromotive power. In measurements, uniaxial pressures are more easily realized than the pressure for the normal mode of bulk distortion, P_3, in Fig. 5. In addition, tensile stresses are not easy to be produced in equipment. Here, we confine ourselves to positive uniaxial pressures (i.e., compressive stresses) for available pressures.

First, we consider a BJT crystal which has a spontaneous contraction $u_3 < 0$ ($c/a < 1$) below $T < T_M$. To this crystal, uniaxial pressures, $P_z(> 0)$, are applied along the tetragonal z axis to enhance $u_3(< 0)$. When, on the other hand, $T > T_M$, the uniaxial pressures produce contractions along the same direction as that of the pressures, so both directions are parallel to the z axis.

Second, we consider another BJT crystal which has a spontaneous elongation $u_3 > 0$ ($c/a > 1$) along the z axis below $T < T_M$. Applications of the pressures $P_z(> 0)$ along the z axis can give rise to a discontinuous conversion of its distortion from $u_3 > 0$ to $u_3 < 0$, when an energy decrease of the crystal by application of $P_{z,\mathrm{tot}}(x)$ may overcome the increase of the anisotropy energy in the $u_2 - u_3$ plane given by Eq. (B4). We do not go into measurements on the phase with $u_3 > 0$ under the positive pressures. When the positive pressures exceed a critical value and/or T is higher than T_M, the positive pressures induce contractions $u_3 < 0$ ($c/a < 1$), whose directions are parallel to that of the pressures, i.e., the z direction.

Irrespective of the sign of the spontaneous u_3 below T_M, therefore, a measurement system is proposed to measure the pressure-gradient electromotive power of BJT crystals with contractions $c/a < 1$ under positive pressures along the z axis. The proposed configuration of the pressures and a BJT crystal set in the circuit shown in Fig. 5 is schematically drawn in Fig. 9(a). The specimen has a shape of a rectangular parallelepiped, which spreads along the x axis from $x = x_1$ to $x = x_2$ under no pressure and has surface planes normal to the tetragonal axis, i.e., the z axis.

A total uniaxial pressure at the position x along the z axis, $P_{z,\mathrm{tot}}(x)$, consists of a uniform pressure $P_z(> 0)$ and a local one $\delta P_z(x)(> 0)$ as follows:

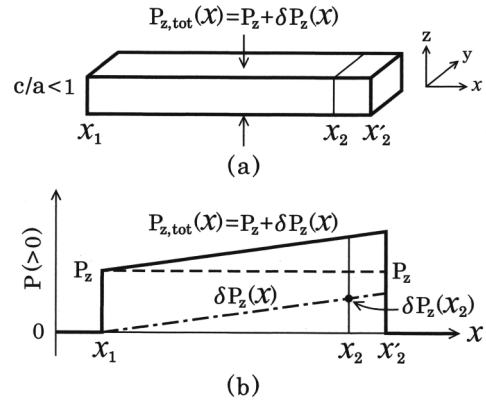

FIG. 9. A measurement system for the pressure-gradient electromotive power $A(P_3, T)$. (a) A rectangular parallelepiped BJT crystal spreads along the x axis from $x = x_1$ to $x = x_2$ under no pressure. The crystal is assumed to have a contraction along the z axis, $c/a < 1$. The uniform and local pressures (compressive stresses), $P_z(> 0)$, and $\delta P_z(x)(> 0)$, respectively, are applied to the crystal along the z axis. The position x_2 is shifted to x_2' by the pressures. (b) The uniform pressure $P_z(> 0)$ is shown by the broken line, while the local pressure $\delta P_z(x)(> 0)$ is shown by the dot-dash line. The local pressure $\delta P_z(x)$ has the constant gradient with respect to x, $[\delta P_z(x_2)/(x_2 - x_1)]$, between x_1 and x_2', where $\delta P_z(x_1) = 0$ is assumed.

$$P_{z,\mathrm{tot}}(x) = P_z + \delta P_z(x). \tag{47}$$

As verified in Eqs. (A6)–(A8), any P_z produces not only P_3 but also P_1. A nonvanishing P_1 does not affect BJT electrons, being neglected. Equations (A8) and (18) give the following equations:

$$\delta P_3(x) = \sqrt{2/3}\, \delta P_z(x), \tag{48}$$

$$\left(\frac{\partial \delta P_3(x)}{\partial x}\right) = \sqrt{\frac{2}{3}}\left(\frac{\partial \delta P_z(x)}{\partial x}\right), \tag{49}$$

$$\left(\frac{\partial \delta u_3(x)}{\partial x}\right) = -\sqrt{\frac{2}{3}}\,\frac{1}{C(P_3, T)}\left(\frac{\partial \delta P_z(x)}{\partial x}\right). \tag{50}$$

In equipment, we produce the local pressure $\delta P_z(x)(> 0)$, which varies linearly with x from $\delta P_z(0) = 0$ at x_1 to $\delta P_z(x_2)$ at x_2. The constant gradient is expressed by

$$\left(\frac{\partial \delta P_z(x)}{\partial x}\right) = \frac{\delta P_z(x_2)}{x_2 - x_1}. \tag{51}$$

The magnitude of $(\partial \delta P_z(x)/\partial x)$ given by Eq. (51) should be small enough to satisfy the condition that the induced $\delta u_3(x)$ can be regarded as an almost constant quantity on a microscopic scale.

The local pressures $\delta P_z(x)$ induce local distortions $\delta u_3(x)$ and $\delta u_1(x)$, which also change the length of the specimen along the x axis to shift the end of the specimen from x_2 to x_2'. Nevertheless, the gradient given by Eq. (51) is conserved between $x = x_1$ and $x = x_2'$. Figure 9(b) shows $\delta P_z(x)$ thus defined together with P_z and $P_{z,\mathrm{tot}}(x)$.

Under the application of the pressures $\delta P_z(x)$ which were elaborated so as to satisfy Eq. (51), the electric field $E_x(x) = E_x$ is determined experimentally by measuring the

electric-potential difference $\Delta\phi$ at the position $x = x_0$, which was shown in Fig. 5. The produced gradient $(\partial\delta P_3(x)/\partial x)$ given by Eqs. (49) and (51) and the measured E_x give the measured pressure-gradient electromotive power $A(P_3, T)$ through Eq. (39). Keep in mind that the experimental P_3 in Eq. (40) is the one evaluated by use of P_z through Eq. (A8).

VII. SUMMARY AND CONCLUDING REMARKS

In BJT metals, some electronic bands are almost degenerate near the Fermi level ϵ_F. This degeneracy is lifted by some bulk uniform distortions which can couple to those electronic bands. A redistribution of electrons in the split bands can decrease the total energy of the redistributed electrons. On the other hand, local distortions which are induced by local pressures change energies of BJT electrons locally and force the BJT electrons to flow in space. These suggest some pressure-electric effects characteristic of BJT metals.

In the present theory, the pressure-electric effect has been studied on the basis of the Γ_{12} subbands, which consist of the two bands labeled $\nu = 2$ and $\nu = 3$ near ϵ_F. When a local pressure with a spatial gradient is applied to induce local distortions, band electrons begin to flow in space. The flows of band electrons are done with suffering electron scatterings by various causes and finally the electron system falls into a steady state. This steady state was obtained by use of the Boltzmann equation together with the relaxation-time approximation. The obtained steady state gives an electromotive power generated by pressures with their gradients, i.e., pressure-gradient electromotive power, to which the two Γ_{12} subbands contribute differently. The pressure-gradient electromotive power becomes nonvanishing in the tetragonal phase, which occurs spontaneously and/or is induced by external uniform pressures.

It is known that the BJT effect always accompanies the elastic softenings [4]. In fact, the experimental observations already verified that the elastic constant $(c_{11} - c_{12})$ is extremely softened in both the cubic and tetragonal phases. Similarly, the elastic constant $C_3(P_3, T)(\approx c_{33} - c_{13})$ is also considerably softened especially at temperatures near the BJT structural-transition temperature T_M. In the crystal with the softened $C_3(P_3, T)$, a local pressure $\delta P_3(x)$ easily produces a large local distortion $\delta u_3(x)$. This consideration has proven that the elastic softening due to BJT effect can strongly enhance the pressure-gradient electromotive power in the BJT metals.

In metals which have weak BJT couplings, the structure of those metals remains to be cubic without the appearance of the structural transition. When such a cubic structure is distorted to be tetragonal by uniform pressures $P_3 \neq 0$, the split Γ_{12}-subbands together with the elastic softening can give the enhanced pressure-gradient electromotive power.

The second-order structural transition considered in the present paper is characteristic of the BJT effect caused by doubly degenerate BJT electronic bands. In the case of a BJT effect by triply degenerate BJT electronic bands, the structural transition is expected to be of the first order [1]. In both BJT effects, however, the structural transitions become of the first order because of the presence of the anharmonic elastic energy. The enhancement of the pressure-gradient electromotive power by the elastic softening becomes conspicuous when structural transitions are close to transitions of the second order which exhibit considerable elastic softenings.

In usual metals, electrons in nondegenerate states around the Γ point near ϵ_F can also exhibit a pressure-electric effect because those electrons can couple linearly to a distortion which has the same symmetry as that of the crystal structure. Since, however, the distortion mode in this case is different from modes of BJT distortion, their pressure-electric effect is insensitive to pressures and temperature without the enhancement of the pressure-gradient electromotive power by the elastic softening due to the BJT effect.

Finally, it is worthwhile to note the following. The obtained pressure-gradient electromotive power results from the flows of electrons pertaining to the BJT effect. The flows are caused by the local BJT distortions, which affect only the BJT subbands. Therefore, the pressure-gradient electromotive power is immediately related to existence of BJT subbands near ϵ_F. Experimental observations of pressure and temperature dependencies of the electromotive power can reveal the BJT subbands existing near ϵ_F. Therefore, the pressure-gradient electric effect can be a probe into the BJT effect, which may work in some metals with structural transitions.

APPENDIX A: UNIAXIAL PRESSURES AND PRESSURES FOR NORMAL MODES OF BULK DISTORTION

In this Appendix, pressures for uniaxial distortions are expressed in terms of pressures for normal modes of bulk distortion.

The elastic energy of a crystal is changed by applying pressures P_2, P_3, and P_1, which induce or enhance the bulk normal modes of distortion u_2 and u_3 given by Eq. (1) and also $u_1 = (e_{xx} + e_{yy} + e_{zz})/\sqrt{3}$. The change in the elastic energy is written as

$$F_P = V(P_1 u_1 + P_2 u_2 + P_3 u_3). \tag{A1}$$

This energy change is rewritten in terms of the uniaxial pressures, P_x, P_y, and P_z as follows:

$$F_P = V(P_x e_{xx} + P_y e_{yy} + P_z e_{zz}). \tag{A2}$$

Comparing Eqs. (A1) and (A2), we obtain

$$P_x = P_1/\sqrt{3} + P_2/\sqrt{2} - P_3/\sqrt{6}, \tag{A3}$$

$$P_y = P_1/\sqrt{3} - P_2/\sqrt{2} - P_3/\sqrt{6}, \tag{A4}$$

$$P_z = P_1/\sqrt{3} + 2P_3/\sqrt{6}. \tag{A5}$$

It is noted that when $P_x = P_y = 0$ and $P_z \neq 0$, we have

$$P_1 = P_z/\sqrt{3}, \tag{A6}$$

$$P_2 = 0, \tag{A7}$$

$$P_3 = P_z/\sqrt{3/2}. \tag{A8}$$

APPENDIX B: EFFECTS OF THE ANHARMONIC ELASTIC ENERGY ON THE STRUCTURAL TRANSITION

The free energy F of a cubic crystal is studied with including the anharmonic elastic energy. We expand F in powers of u_2 and u_3 at temperatures T near a second-order transition temperature $T_{\rm M}$. The resultant F can be written as follows:

$$F = V\left\{\frac{1}{2}a_2\left(\frac{T-T_{\rm M}}{T_{\rm M}}\right)\left(u_2^2+u_3^2\right) + \frac{2}{3}a_3\left(u_3^3-3u_2^2u_3\right)+\frac{1}{4}a_4\left(u_2^2+u_3^2\right)^2\right\}, \tag{B1}$$

where $a_2(>0)$, a_3, and $a_4(>0)$ are the expansion coefficients independent of T.

In Eq. (B1), the term of $(u_3^3-3u_2^2u_3)$ is the anharmonic elastic energy. This energy is anisotropic in the u_2-u_3 plane, so the equilibrium distortion below the transition temperature is uniquely determined as follows:

$$u_3<0 \text{ and } u_2=0 \text{ for } a_3>0, \tag{B2}$$

$$u_3>0 \text{ and } u_2=0 \text{ for } a_3<0. \tag{B3}$$

The anisotropy energy in the u_2-u_3 plane, i.e., the difference between the energy of a BJT crystal with $u_3>0$, $F_{u_3>0}$ and that with $u_3<0$, $F_{u_3<0}$ is expressed by

$$F_{u_3>0}-F_{u_3<0}=(4/3)Va_3|u_3|^3. \tag{B4}$$

When $u_2=0$, the presence of the u_3^3 term causes a first order transition of u_3, which has a transition temperature $T_{\rm M1}$. The conditions for the first-order transition at $T_{\rm M1}$,

$$\left(\frac{\partial F}{\partial u_3}\right)=0 \text{ and } F=0 \text{ at } u_3\neq 0, \tag{B5}$$

determine $T_{\rm M1}$ as follows:

$$T_{\rm M1}\sim\left(1+\frac{2a_3^2}{3a_2a_4}\right)T_{\rm M}. \tag{B6}$$

On the other hand, the elastic constant $C_3(0,T)$ at $T=T_{\rm M1}$ in the tetragonal phase is obtained to be

$$C_3(0,T_{\rm M1})=\frac{1}{V}\left(\frac{\partial^2F}{\partial u_3^2}\right)_{T\to T_{\rm M1}-0} \sim 2a_3^2/a_4. \tag{B7}$$

This equation shows that $C_3(0,T_{\rm M1})$ becomes nonvanishing at $T_{\rm M1}$ because of the presence of the anharmonic elastic energy.

APPENDIX C: A NUMERICAL CONSIDERATION ON THE PRESSURE-GRADIENT ELECTROMOTIVE POWER

Using available observed data together with the Γ_{12} subband model, we make a numerical consideration on $A(P_3,T)$ given by Eqs. (44) and (41) in the case of Nb_3Sn. The observed BJT distortion of this metal is $c/a-1=-6.2\times10^{-3}$ [20], which gives $u_3\approx-5.0\times10^{-3}$. This distortion causes the splitting of the BJT subbands, $2\sqrt{c_0v_{\rm c}}g_0u_3$, which is estimated to be 6.3 mRy by using the result of the electronic band calculation [24]. These two values give $\sqrt{c_0v_{\rm c}}g_0\approx8.5$ eV.

On the other hand, the temperature dependence of $(c_{11}-c_{12})$ in the cubic phase was measured on Nb_3Sn [25]. Extrapolating the measured values of $(c_{11}-c_{12})$ to a value at high temperatures, we employ $c_0\approx1.5\times10^{11}\,{\rm N/m^2}$. The values of $\sqrt{c_0v_{\rm c}}g_0$ and c_0 thus obtained are used to estimate $\sqrt{(v_{\rm c}/c_0)}g_0$ in Eq. (41). Finally, we arrive at

$$A(P_3.T)=-(5.6\times10^{-11}\ {\rm V\,m^2/N})\times\frac{1}{\lambda}\left\langle\left\langle\frac{A(P_3,T)}{A_0}\right\rangle\right\rangle. \tag{C1}$$

In this equation, $\langle\langle A(P_3,T)/A_0\rangle\rangle$ is $A(P_3,T)/A_0$ calculated by use of Eq. (44) and was shown in Figs. 6–8 but only for $\alpha=1.08$ or 0.98. It is noted that $\langle\langle A(P_3,T)/A_0\rangle\rangle>0$. Further, it is probable that $\lambda=O(10^0)$.

[1] P. J. Labbé and J. Friedel, J. Phys. France **27**, 153 (1966); P. J. Labbé and J. Friedel, J. Phys. France **27**, 303 (1966).

[2] B. M. Klein, L. L. Boyer, D. A. Papaconstantopoulos, and L. F. Mattheiss, Phys. Rev. B **18**, 6411 (1978).

[3] M. Kataoka, Phys. Lett. A **80**, 35 (1980).

[4] M. Kataoka, Phys. Rev. B **28**, 2800 (1983).

[5] M. Weger and I. B. Goldberg, in *Solid State Physics*, edited by H. Ehrenreich, F. Seiz, and D. Turnbull (Academic, New York, 1973), Vol. 28, p. 1.

[6] Yu. A. Izyumov and Z. Z. Kurmaev, Sov. Phys. Usp. **17**, 356 (1974).

[7] C. C. Yu and P. W. Anderson, Phys. Rev. B **29**, 6165 (1984).

[8] A. N. Vasil'ev, V. D. Buchel'nikov, T. Takagi, V. V. Khovailo, and É. I. Éstrin, Phys. Usp. **46**, 559 (2003).

[9] P. Entel, A. Dannenberg, M. Siewert, H. C. Herper, M. E. Gruner, V. D. Buchelnikov, and V. A. Chernenko, Mater. Sci. Forum **684**, 1 (2011).

[10] S. Fujii, S. Ishida, and S. Asano, J. Phys. Soc. Jpn. **58**, 3657 (1989).

[11] P. J. Brown, A. Y. Bargawi, J. Crangle, K.-U. Neumann, and K. R. A. Ziebeck, J. Phys.: Condens. Matter **11**, 4715 (1999).

[12] M. Ye, A. Kimura, Y. Miura, M. Shirai, Y. T. Cui, K. Shimada, H. Namatame, M. Taniguchi, S. Ueda, K. Kobayashi, R. Kainuma, T. Shishido, K. Fukushima, and T. Kanomata, Phys. Rev. Lett. **104**, 176401 (2010).

[13] A. Chakrabarti, M. Siewert, T. Roy, K. Mondal, A. Banerjee, M. E. Gruner, and P. Entel, Phys. Rev. B **88**, 174116 (2013).

[14] M. Zelený, A. Sozinov, L. Straka, T. Björkman, and R. M. Nieminen, Phys. Rev. B **89**, 184103 (2014).

[15] A. K. Verma and P. Modak, Europhys. Lett. **81**, 37003 (2008).

[16] M. D. Kaplan and B. G. Vekhter, *Cooperative Phenomena in Jahn-Teller Crystals* (Plenum Press, New York, 1995).

[17] I. B. Bersuker, *The Jahn-Teller Effect* (Cambridge University Press, Cambridge, 2006).

[18] G. L. Bir and G. E. Pikus, *Symmetry and Strain-Induced Effects in Semiconductors* (Wiley, New York, 1974).
[19] M. Kataoka and J. Kanamori, J. Phys. Soc. Jpn. **32**, 113 (1972).
[20] R. Mailfert, B. W. Batterman, and J. J. Hanak, Phys. Lett. A **24**, 315 (1967).
[21] B. W. Batterman and C. B. Barrett, Phys. Rev. **145**, 296 (1966).
[22] H. Ibach and H. Brüth, *Festkörperphysik* (Springer-Verlag, Berlin, Heidelberg, 1995)
[23] J. M. Ziman, *Principles of the Theory of Solids* (Cambridge University Press, London, 1964).
[24] W. Weber and L. F. Mattheiss, Phys. Rev. B **25**, 2270 (1982).
[25] K. R. Keller and J. J. Hanak, Phys. Rev. **154**, 628 (1967).